

**Hot phonon effects on the high-field transport in metallic carbon nanotubes**

Christoph Auer\* and Ferdinand Schürer†

*Institute of Theoretical and Computational Physics, Graz University of Technology, Petersgasse 16, 8010 Graz, Austria*

Christian Ertler‡

*Institute of Theoretical Physics, University of Regensburg, Universitätsstraße 31, 93053 Regensburg, Germany*

(Received 25 April 2006; revised manuscript received 31 July 2006; published 23 October 2006)

We present a kinetic transport model for hot electrons and hot phonons in metallic single-wall carbon nanotubes. The transport model is based on a coupled system of Boltzmann equations of linearly dispersive electrons and optical phonons. An efficient and accurate deterministic numerical scheme is developed to solve the set of kinetic equations. With this numerical tool we study in detail the high-field transport properties of ohmically contacted molecular nanotube wires lying on a substrate. The simulations demonstrate that the optical phonons are strongly driven out of thermal equilibrium. Nonequilibrium optical phonons are found to influence considerably the electron transport in the high-field regime. We observe that the steady-state current at high bias is sensitive to the anharmonic lifetime of the optical phonons and to the phonon group velocities. Comparisons of experimental current-voltage characteristics with the theoretical results obtained with electron-phonon coupling coefficients as predicted by density functional calculations exhibit very good agreement.

DOI: [10.1103/PhysRevB.74.165409](https://doi.org/10.1103/PhysRevB.74.165409)

PACS number(s): 73.61.Wp, 73.50.Fq, 72.10.Di

**I. INTRODUCTION**

Single-wall carbon nanotubes (SWCNT's) have become increasingly interesting for the development of electronic applications on the nanoscale. Depending on their atomic structure, SWCNT's are semiconductors or metals.<sup>1</sup> Active electronic devices such as carbon nanotube field-effect transistors<sup>2-4</sup> can be fabricated from semiconducting SWCNT's. On the other hand, metallic nanotubes are prototypes of one-dimensional (1D) conductors<sup>5-7</sup> that can be used to realize interconnects in integrated circuits. The main reasons for the attractiveness of SWCNT's as future electronic devices are the observed ballistic electron transport and the high current densities that can be carried before they break.<sup>6,8,9</sup> Recent studies<sup>10-12</sup> show that ballistic transport up to a few hundred nanometers is possible only for small applied voltages  $U < 0.2$  V. In the case of high bias, the current saturates in long tubes and is significantly reduced in short tubes due to inelastic electron scattering caused by optical phonons. Very recently, it has been shown that the high-field current in suspended nanotubes is even lower than in SWCNT's lying on a substrate.<sup>13,14</sup> Furthermore, long suspended nanotubes exhibit negative differential conductance<sup>13,14</sup> resulting from reinforced electron scattering caused by heated nonequilibrium phonons. The interaction between electrons and optical phonons in SWCNT's is very strong. Accurate density functional theory (DFT) calculations predict an optical mean free path (MFP) of  $l_{op} \approx 65d$  for tube diameters  $d$  between 1 and 3 nm.<sup>15</sup> These results have been confirmed by experimental determinations of the electron-phonon coupling (EPC) based on measurements of phonon dispersions and Raman  $D$  peak dispersions.<sup>16,17</sup> However, MFP's which are ten times lower must be assumed to recover the measured current voltage characteristics in transport calculations.<sup>10-14</sup> For the development of high performance nanotube electronics, it is essential to understand what ultimately limits the current in SWCNT's. Hence, an adequate transport model is required to investigate the fun-

damental transport properties of nanotubes in the high-field regime.

So far, theoretical investigations of the high-field transport in metallic SWCNT's have been carried out at the kinetic level by solving the semiclassical Boltzmann equation of electrons<sup>10,11</sup> and at a macroscopic level by modeling the resistance as a function of the applied bias and the phonon temperatures.<sup>11-14</sup> The transport equations considered in Refs. 10 and 11 rely on the assumption of phonons in equilibrium at a fixed lattice temperature. Recently, Lazzeri *et al.*<sup>15</sup> have pointed out that optical phonons are far from equilibrium at high applied fields. Starting from the EPC values presented in Refs. 15 and 16, they show that phonon occupations in the range of 3-5 (Ref. 15) result in optical MFP's of  $l_{op} \approx 10$  nm as obtained from the transport calculations.<sup>10-12</sup> These phonon occupations of the optical modes imply effective temperatures of  $T > 6000$  K. In Refs. 13 and 14, simple macroscopic approaches are presented to include the self-heating effect in suspended SWCNT's. Nonequilibrium effects of the optical phonon system are incorporated by considering an effective temperature for optical phonons different from the lattice temperature. However, studies of strongly coupled electron-phonon systems in polar semiconductors prove that their transport properties are strongly influenced by the nonequilibrium shape of the phonon distributions.<sup>18-21</sup> If strong kinetic effects occur, transport models based on equilibrium phonon distributions with effective temperatures become very inaccurate.<sup>19,21</sup> Hence, we suggest that the electron transport in SWCNT's under high bias must be entirely treated at the kinetic level and must include the nonequilibrium dynamics of optical phonons.

In this paper, we propose a transport model for metallic SWCNT's based on a coupled system of semiclassical Boltzmann equations of electrons and optical phonons. In this way, the influence of the nonequilibrium behavior of the phonon distributions on the electron transport is taken into account dynamically. We present a deterministic numerical method to obtain accurate transient solutions of the consid-

ered transport equations. With the help of this numerical tool, simulations of the high-field electron transport in ohmically contacted SWCNT's of different length and width are performed. The considered nanotubes are in thermal contact with the substrate on which they are grown. We demonstrate that the proposed transport model is able to reproduce measured current voltage characteristics of metallic SWCNT's by using EPC strengths consistent with those obtained from DFT calculations. Our calculations show that the optical phonons are driven far from equilibrium at high applied bias, especially at the contact boundaries. This nonequilibrium behavior of the optical phonons is found to influence significantly the electron transport. The impact of the nonequilibrium phonons on the electron system is systematically studied by varying the anharmonic lifetime of the optical phonons and by comparing the results with calculations based on equilibrium phonon distributions with adapted effective temperatures.

The rest of the paper is organized as follows. In Sec. II, we introduce the kinetic model and discuss its main physical aspects. The numerical method for solving the coupled system of Boltzmann equations is briefly described in Sec. III. In Sec. IV, we present the numerical results of the performed transport simulations. Finally, concluding remarks are drawn in Sec. V.

## II. KINETIC MODEL

SWCNT's are identified by their chiral vector  $C_h = na_1 + ma_2$ , where  $a_1$  and  $a_2$  denote the graphene lattice vectors.<sup>1</sup> The integers  $n$  and  $m$  are called the chiral indices. A nanotube with chiral vector  $C_h$  is obtained by rolling up a strip of graphene in the direction of  $C_h$  so that the atoms connected by  $C_h$  coincide. The resulting SWCNT has a periodic structure along its axis. For nanotubes with diameter  $d \geq 1$  nm, the electron states  $\kappa$  and their energy  $\varepsilon(\kappa)$  can be deduced from the band structure of graphene by imposing periodic boundary conditions in the circumferential direction.<sup>1</sup> According to this zone-folding principle, the allowed Bloch vectors  $\kappa$  of electrons form a set of equidistant parallel lines in the 2D reciprocal space. The graphene energy bands split into a series of subbands that determine the 1D band structure of the nanotube.<sup>1</sup>

In the following, we concentrate on so-called armchair nanotubes characterized by equal chiral indices,  $n=m$ . For symmetry reasons, the allowed electron states of armchair nanotubes with arbitrary  $n$  contain the two equivalent points  $\mathbf{K}$  and  $\mathbf{K}'=2\mathbf{K}$  (Ref. 1). Since the valence and conduction band of graphene touch at these symmetry points, armchair nanotubes are 1D metals. At each point  $\mathbf{K}$  and  $\mathbf{K}'$ , the electron energies  $\mathcal{E}(\kappa) - \mathcal{E}_F$  near the Fermi level  $\mathcal{E}_F$  are well approximated by the linear dispersion relations

$$\varepsilon_i(k) = \hbar v_i k, \quad i = 1, 2 \quad (1)$$

with positive  $v_1 = +v_F$  and negative  $v_2 = -v_F$  Fermi velocities.<sup>15</sup> In Eq. (1),  $\hbar$  is the reduced Plank constant  $h/2\pi$  and the variable  $k$  denotes the components along the tube axis of the momentum vectors  $\kappa - \mathbf{K}$  and  $\kappa - \mathbf{K}'$ , respectively. Electrons in these states can be considered as equivalent car-

riers in the transport model. Hence, it is sufficient to introduce the two phase-space distribution functions  $f_i(\varepsilon, x, t)$  with  $i$  referring to right ( $i=1$ ) and left moving ( $i=2$ ) electrons.<sup>10</sup> The distribution functions  $f_i(\varepsilon, x, t)$  depend on the energy  $\varepsilon = \varepsilon_i(k)$ , the position variable  $x$  and time  $t$ . All further semiconductorlike energy subbands of the nanotube are neglected, which is valid for electrons with energies  $|\varepsilon| < 2\hbar v_F/d$ . Assuming a tube diameter of  $d=2$  nm, this energy bound is approximately 0.55 eV.

The temporal evolution of the distribution functions  $f_i = f_i(\varepsilon, x, t)$  is governed by the Boltzmann equations

$$\partial_t f_i + v_i \partial_x f_i - e_0 v_i E \partial_\varepsilon f_i = C_i, \quad (2)$$

where  $e_0$  denotes the electron charge and  $E$  the electric field along the tube axis. The collision operator  $C_i$  on the right-hand side of Eq. (2) determines the temporal changes of  $f_i$  due to electron scattering. First, we take into account the interaction of electrons with acoustic phonons in terms of elastic back-scattering processes. For the corresponding collision operator, we obtain

$$C_i^{ac} = \frac{v_F}{l_{ac}} (f_j - f_i), \quad (3)$$

with  $j \neq i$  and the acoustic mean free path  $l_{ac}$ .<sup>10</sup> It should be mentioned that the effect of electron scattering at impurities can be included by substituting the elastic MFP  $l_e = 1/(1/l_{ac} + 1/l_{im})$  for  $l_{ac}$  in Eq. (3). Here,  $l_{im}$  denotes the MFP due to impurity scattering.

The elastic scattering processes mainly determine the conductance of the nanotube in the low bias regime. If high electric fields are applied, the current is essentially limited by inelastic interactions of electrons with optical phonons. The application of Fermi's golden rule leads to<sup>15</sup>

$$s_{ij}(k) = \frac{2\pi}{\hbar} \sum_{\eta} \int_B dq |c_{jk+q,ik}^{\eta}|^2 \times \{g_{\eta}(q) \delta[\varepsilon_i(k) - \varepsilon_j(k+q) + \hbar\omega_{\eta}(q)] + [g_{\eta}(-q) + 1] \times \delta[\varepsilon_i(k) - \varepsilon_j(k+q) - \hbar\omega_{\eta}(-q)]\} \quad (4)$$

for the scattering rate of electrons in the state  $(i, k)$  due to absorption and emission of phonons with wave vectors  $q$  and  $-q$ . In the latter equation we have introduced the phonon distribution function  $g_{\eta}(q)$  for the mode  $\eta$  and the phonon energy  $\hbar\omega_{\eta}(q)$ . The electron-phonon coupling (EPC) is determined by the quantity  $c_{jk',ik}^{\eta}$ . The scattering rate Eq. (4) is obtained by using Fermi's golden rule, which is the standard method of lattice scattering in semiconductors.<sup>22</sup> This approach is valid if the electron-phonon interaction can be treated as perturbation of the noninteracting system and if the temporal changes of the distribution functions are small within the duration of a collision event. The magnitudes of the EPC and the scattering rates for electrons in metallic SWCNT's (Ref. 15) are similar to that of electrons in semiconductors.<sup>22,23</sup> Hence, we conclude that the scattering rates based on Fermi's golden rule can also be applied in the case of SWCNT's. According to Ref. 15, we consider three different types of interaction between optical phonons and

electrons with energies near the Fermi level. The most efficient interaction is the back-scattering of electrons due to phonons of the  $\mathbf{K}-A_1'$  mode with wave vectors  $\mathbf{q} \approx \mathbf{K}$ . These phonons are often called K phonons or zone-boundary phonons. Furthermore, longitudinal optical (LO) and transverse optical (TO)  $\Gamma$  phonons with small  $|q|$  cause back-scattering and forward-scattering of electrons. In the following, we use the mode indices  $\eta=1,2,3$  when referring to K phonons, LO  $\Gamma$  phonons, and TO  $\Gamma$  phonons, respectively. We point out that the dispersion of the optical phonons is much smaller than the dispersion of electrons. Therefore, we assume constant phonon frequencies  $\omega_\eta$  for the evaluation of the scattering rate (4). Further, the quantities  $|c_{jk+q,ik}^\eta|^2$  determining the EPC are considered to be independent of  $k$  and  $q$  for the scattering of electrons with energies near the Fermi energy. Hence, the collision operators modeling back scattering due to phonons of the modes  $\eta=1,2$  read

$$\begin{aligned} C_i^\eta = & \gamma_\eta \{ g_\eta(q_i^-) f_j^-(1-f_i) + [g_\eta(q_i^+) + 1] f_j^+(1-f_i) \\ & - g_\eta(q_i^+) f_i(1-f_j^+) - [g_\eta(q_i^-) + 1] f_i(1-f_j^-) \}, \end{aligned} \quad (5)$$

with  $j \neq i$  and the EPC constants  $\gamma_\eta$ . In Eq. (5), we use the abbreviations  $f_i = f_i(\varepsilon, x, t)$ ,  $f_i^\pm = f_i(\varepsilon \pm \hbar\omega_\eta, x, t)$ , and

$$q_i^\pm = \mp \frac{1}{\hbar v_i} (2\varepsilon \pm \hbar\omega_\eta). \quad (6)$$

The collision operator  $C_i^3$ , which takes into account the forward scattering of electrons, has the same formal structure as the operators in Eq. (5). However, the phonon wave vectors  $q_i^\pm$  are determined by  $q_i^+ = q_i^- = q_i = \omega_3/v_i$  in the case of forward scattering. Finally, the total electron scattering operator on the right-hand side of the Boltzmann equation (2) results in

$$C_i = C_i^{ac} + \sum_{\eta=1}^3 C_i^\eta. \quad (7)$$

The investigations of the electron transport in metallic SWCNT's presented in Refs. 10–12 assumed optical phonons in equilibrium at a fixed lattice temperature  $T$ . This means that  $g_\eta(q)$  is set equal to the Bose-Einstein distribution  $g_\eta^0 = 1/[\exp(\hbar\omega_\eta/k_B T) - 1]$ , where  $k_B$  is the Boltzmann constant. The phonon energies for K and  $\Gamma$  phonons are  $\hbar\omega_1 \sim 161.2$  meV and  $\hbar\omega_2 = \hbar\omega_3 \sim 196.0$  meV.<sup>15</sup> At room temperature we obtain  $g_\eta^0 \ll 1$  for the Bose-Einstein distributions. For this reason, electron scattering due to phonon absorption processes was neglected in the earlier studies.<sup>10–12</sup> In the present work, we go beyond these approaches and treat the phonon distribution functions as unknowns of an extended kinetic model for electrons and optical phonons in SWCNT's. We consider the phonon distribution functions  $g_\eta(q, x, t)$  to depend on the 1D wave vector  $q$ , on the position  $x$  and on time  $t$ . It will be shown in Sec. IV that  $g_\eta(q, x, t)$  takes on much larger values than the equilibrium distribution  $g_\eta^0$  in the high-field regime. Since in general  $g_\eta(q, x, t) \geq 1$  occurs, it is essential to include electron scattering due to both absorption and emission processes in the collision operators (5). The temporal evolution of the phonon distribution functions is determined by the Boltzmann equations

$$\partial_t g_\eta + v_\eta \partial_x g_\eta = \mathcal{D}_\eta, \quad (8)$$

with the phonon velocities  $v_\eta = \partial_q \omega_\eta$  and the phonon collision operators  $\mathcal{D}_\eta$ . As mentioned before, we neglect the phonon dispersion for the evaluation of the electron scattering operators (5). However, nonzero phonon velocities  $v_\eta$  are considered in Eq. (8) to incorporate the effect of spatial diffusion of optical phonons. According to Ref. 16, the dispersion of  $\Gamma$  and K phonons in graphene is linear for small  $|q|$ , i.e.,  $\omega_{\Gamma\text{LO/TO}}(\mathbf{q}) = \omega_{\Gamma\text{LO/TO}}(\mathbf{0}) + \alpha_{\Gamma\text{LO/TO}}|q|$  and  $\omega_{\mathbf{K}}(\mathbf{K} + \mathbf{q}) = \omega_{\mathbf{K}}(\mathbf{K}) + \alpha_{\mathbf{K}}|q|$  with slopes  $\alpha_{\Gamma\text{LO}} \sim 157$  cm<sup>-1</sup> Å,  $\alpha_{\Gamma\text{TO}} \sim 0$  and  $\alpha_{\mathbf{K}} \sim 384$  cm<sup>-1</sup> Å. Hence, the phonon velocities are  $|v_1| \sim 7230$  m/s,  $|v_2| \sim 2950$  m/s, and  $|v_3| \sim 0$ .

The phonon collision operators consist of the two terms  $\mathcal{D}_\eta = \mathcal{D}_\eta^{ep} + \mathcal{D}_\eta^{pp}$ , where the first one stems from the electron-phonon interaction and the second one allows for phonon-phonon interaction processes. In the case of back-scattering phonons, we obtain

$$\begin{aligned} \mathcal{D}_\eta^{ep} = & 2 \sum_{i=1}^2 \gamma_\eta \{ (g_\eta + 1) f_i(\varepsilon_i^+) [1 - f_j(\varepsilon_i^-)] \\ & - g_\eta f_j(\varepsilon_i^-) [1 - f_i(\varepsilon_i^+)] \} \end{aligned} \quad (9)$$

for  $\eta=1,2$  and  $j \neq i$ . Here, we use the abbreviations  $g_\eta = g_\eta(q, x, t)$ ,  $f_i(\varepsilon_i^\pm) = f_i(\varepsilon_i^\pm, x, t)$  with  $\varepsilon_i^\pm = \hbar(v_i q \pm \omega_\eta)/2$ . When deriving the collision terms (9), one must take into account that the left and right moving electrons are four times degenerate (two spin components at  $\mathbf{K}$  and  $\mathbf{K}'$ ). The electron-phonon collision operator for the phonon mode  $\eta=3$  reads

$$\begin{aligned} \mathcal{D}_3^{ep} = & \gamma_3 \sum_{i=1}^2 J_i \delta_{q, q_i} \int_{\mathbb{R}} d\varepsilon \{ (g_3 + 1) f_i(\varepsilon) [1 - f_i(\varepsilon^-)] \\ & - g_3 f_i(\varepsilon^-) [1 - f_i(\varepsilon)] \}, \end{aligned} \quad (10)$$

with  $\varepsilon^- = \varepsilon - \hbar\omega_3$ . The quantity  $J_i = 4L/(hv_F)$  denotes the density of states for electrons of type  $i$ , and  $L$  the tube length. The space and time variables  $x$  and  $t$  of the distribution functions in Eq. (10) are omitted for brevity. Due to the Kronecker delta  $\delta_{q, q_i}$  in the collision operator (10), only phonons with the wave vectors  $q_i = \omega_3/v_i$  are emitted and absorbed by forward scattering of electrons. This is a consequence of the linear dispersion of electrons and the constant phonon frequency.

Phonon-phonon interactions are treated in relaxation time approximation, which leads to the collision operator

$$\mathcal{D}_\eta^{pp} = - \frac{1}{\tau_\eta} [g_\eta(q, x, t) - g_\eta^0], \quad (11)$$

with the relaxation time  $\tau_\eta$ . The Bose-Einstein distribution  $g_\eta^0$  is evaluated at a fixed lattice temperature  $T$ . The quantity  $\tau_\eta$  is the phonon lifetime determined by the anharmonic contributions to the interatomic potential. Measurements of the linewidths of Raman  $G^+$  peaks in metallic nanotubes predict  $\gamma^{an} \sim 10$  cm<sup>-1</sup> for the anharmonic contribution.<sup>17</sup> This implies a lifetime of  $\tau^{an} \sim 3.3$  ps.

Our aim is to investigate the electron transport in ohmically contacted SWCNT's of finite length. Hence, we must impose proper boundary conditions at  $x=0$  and  $x=L$  for this

open system. Since the Boltzmann equations (2) and (8) are hyperbolic conservation laws, we must consider only inflow boundary conditions. This means that we fix the values of the distribution functions for right moving particles at  $x=0$  and for left moving particles at  $x=L$ . As boundary condition for electrons at the left contact, e.g., we use

$$f_1(\varepsilon, x=0, t) = t_1^2 f^0(T) + (1 - t_1^2) f_2(\varepsilon, x=0, t), \quad (12)$$

where  $t_1^2$  is the transmission coefficient of the contact and  $f^0(T) = [1 + \exp(\varepsilon/k_B T)]^{-1}$  denotes the Fermi-Dirac distribution. Hence, we assume that electrons that enter the nanotube from the contact are in equilibrium at the temperature  $T$ . Regarding the optical phonons, we consider the inflow boundary conditions  $g_\eta(q, x=0, t) = g_\eta^0$  for  $v_\eta(q) > 0$  and  $\eta = 1, 2$ . Corresponding boundary conditions are assumed at the right contact.

The set of Boltzmann equations (2) and (8) constitutes a kinetic transport model that fully includes the dynamics of optical phonons. This allows us to study the transient far-from-equilibrium behavior of the electron-phonon system in metallic SWCNT's. In the next section, we describe a numerical method for solving the transport equations (2) and (8).

### III. NUMERICAL METHOD

Simulations of the carrier transport at the kinetic level are usually performed by applying the Monte Carlo technique.<sup>24,25</sup> Recently, deterministic solution methods for Boltzmann type equations have been developed<sup>20,21,26,27</sup> and successfully applied to simulate the transport properties of submicron semiconductor devices. The main advantage of the deterministic approach over the Monte Carlo technique is that the distribution functions can be directly calculated without statistical noise. Compared to the simulation of classical semiconductor devices, such as a silicon MOSFET, the investigation of the electron transport in SWCNT's is a low-dimensional problem. The distribution functions  $f_i(\varepsilon, x, t)$  and  $g_\eta(q, x, t)$  depend on only two phase-space variables. Therefore, the kinetic transport model defined by the Boltzmann equations (2) and (8) can be solved very efficiently with the help of a deterministic solver.

The developed numerical method is based on a fixed uniform discretization of the phase-space variables  $x$ ,  $\varepsilon$ , and  $q$ . First, the discretization length  $\Delta\varepsilon$  of the energy variable is chosen so that the phonon energies  $\hbar\omega_\eta$  are integer multiples of  $\Delta\varepsilon$ , i.e.,  $\hbar\omega_\eta = \sigma_\eta \Delta\varepsilon$  with  $\sigma_\eta \in \mathbb{N}$ . The energy grid is determined by the values  $\varepsilon_n = -\hat{\varepsilon} + n\Delta\varepsilon$  for  $n=0, \dots, N$  with the maximal energy  $\hat{\varepsilon} = \Delta\varepsilon N/2$ . Starting from this discretization, we define the grid points  $q_m^\eta = -\hat{q}^\eta + m\Delta q$  for  $m=0, \dots, N - \sigma_\eta$  with  $\Delta q = 2\Delta\varepsilon/\hbar v_F$  and  $\hat{q}^\eta = \Delta q(N - \sigma_\eta)/2$  for the wave vector of the phonon modes  $\eta=1, 2$ . These discretizations of  $\varepsilon$  and  $q$  guarantee that the energy and momentum relations  $\varepsilon(k') = \varepsilon(k) \pm \hbar\omega_\eta$  and  $k' = k \pm q$  are satisfied at a discrete level in each individual back-scattering process. Hence, the collision operators (7) and (9) can be evaluated exactly in terms of the discretized distribution functions  $f_i(x, \varepsilon_n, t)$  and  $g_\eta(x, q_m^\eta, t)$ . This is a major advantage compared to approxi-

mative evaluations of the collision operators with the Monte Carlo method. It should be noted that in the stochastic treatment, the factors  $1-f_i$  of the collision operators must be approximated from the electron ensemble in each time step.<sup>11</sup> In the case of forward scattering, we must only take into account the two phonon wave vectors  $q_i = \omega_3/v_i$  with  $i=1, 2$ . The integrals with respect to  $\varepsilon$  in the collision operator (10) are carried out in an efficient way by applying the midpoint rule.

From a mathematical point of view, the left-hand sides of Eqs. (2) and (8) are hyperbolic conservation laws. We therefore apply a conservative high-order finite-difference scheme to approximate the derivatives with respect to  $x$ ,  $\varepsilon$ , and  $q$  in the Boltzmann equations and (2) and (8). According to this method, the derivative  $\partial_\varepsilon f_i$ , e.g., is approximated by

$$\partial_\varepsilon f_i(x, \varepsilon_n, t) \approx \frac{1}{\Delta\varepsilon} [F_{in+1/2}(x, t) - F_{in-1/2}(x, t)], \quad (13)$$

where  $F_{in+1/2}(x, t)$  are the so-called numerical fluxes. In the framework of weighted essentially nonoscillatory (WENO) schemes,<sup>28</sup> these quantities are obtained in terms of the discretized distribution functions  $f_i(x, \varepsilon_n, t)$  by applying a high-order nonlinear polynomial reconstruction. We use a fifth-order version of the WENO method<sup>28</sup> that has already been successfully applied to solve the semiconductor Boltzmann equation.<sup>26</sup>

The phase-space discretization of the coupled BTE's for electrons and phonons finally results in a system of ordinary differential equations (ODE's), which determines the temporal evolution of the distribution functions evaluated at the grid points. A stable time integration of this system of ODE's can be performed with the help of the explicit total variation diminishing (TVD) Runge-Kutta type schemes.<sup>29</sup> We applied the second-order version presented in Ref. 29, which is equivalent to Heun's method.

In order to test and validate the developed numerical scheme, we performed simulations of the electron transport in metallic SWCNT's under different physical conditions. Due to our deterministic approach, the main errors of the phase-space discretization arise from approximating the derivatives of  $f_i$  at the left-hand side of the Boltzmann equation. Hence, we first studied the ballistic electron transport by solving Eq. (2) with  $C_i=0$ . In the ballistic case, the exact result for the steady-state current is  $J_{th} = 4e_0^2 U/h$ , where  $U$  denotes the applied bias. The comparison of the numerically obtained current  $J$  with  $J_{th}$  exhibits a very small error of  $|J - J_{th}|/J_{th} \approx 10^{-7}$  for discretization lengths  $\Delta\varepsilon = 40$  meV and  $\Delta x = 20$  nm. This shows that highly accurate results can be obtained with rather coarse grids. To test the numerical method in presence of electron-phonon interactions, we repeated the transport simulation presented in Ref. 10 for a one micron long metallic SWCNT. Hence, we used the same transport model as in Ref. 10 and considered only back scattering of electrons due to acoustic phonons and due to emission of optical phonons in equilibrium at a fixed lattice temperature. A comparison of the current obtained in our calculation with the results of Yao *et al.*<sup>10</sup> is presented in Fig. 1. Excellent agreement between the data is obtained with the

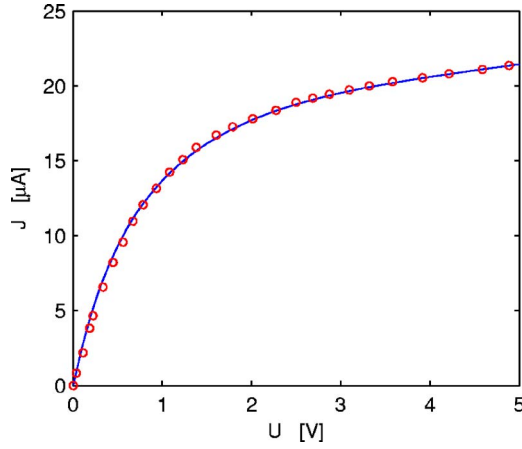


FIG. 1. (Color online) Current  $J$  versus applied voltage  $U$  for a one micron long SWCNT. The symbols  $\circ$  display the theoretically obtained data of Yao (Ref. 10) and the solid line represents our results.

same grid as in the ballistic case. It should be mentioned that the results shown in Fig. 1 stem from calculations based on linear approximations of the band structure. The higher semiconductorlike electron bands are neglected in both cases. We point out that this approximation is not justified for bias voltages  $U > 1.5$  V. The comparison of the results for  $U > 1.5$  V displayed in Fig. 1 is only considered as test of the numerical scheme. The performed numerical tests show that the proposed numerical method is very well suited for solving kinetic equations such as (2) and (8).

#### IV. TRANSPORT SIMULATIONS

In this section, we study the steady-state transport properties of metallic SWCNT's. The numerical method introduced above is designed to calculate the transient solution of the Boltzmann equations (2) and (8) of electrons and phonons. We obtain the steady state results from this transient solution by performing the time integration until the distribution functions show a temporal stabilization. As criteria for reaching the stationary state we considered the two conditions

$$\begin{aligned} |\bar{J}(t) - \bar{J}(t - \Delta_t)| &< \epsilon_t |\bar{J}(t)|, \\ |\max_x [J(x,t)] - \min_x [J(x,t)]| &< \epsilon_x |\bar{J}(t)|, \end{aligned} \quad (14)$$

to be satisfied simultaneously by the electron current  $J(x,t)$ . The first condition imposes a bound on the temporal change of the space-averaged current  $\bar{J}(t)$  within the time interval  $\Delta_t$ . The second one limits the spatial variation of the current which determines the temporal derivative of the electron density in the 1D case. For the calculations presented in the following, we used  $\Delta_t = 1.0$  ps and  $\epsilon_t = \epsilon_x = 10^{-3}$ .

##### A. Comparison with experimental results

In Fig. 2, we compare the results of our transport simulations with the measured current-voltage characteristics of

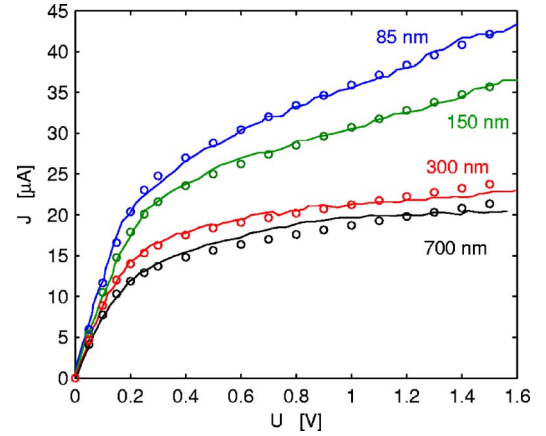


FIG. 2. (Color online) Current-voltage (J-U) characteristics of ohmically contacted SWCNT's of different lengths and diameters  $d \sim 2-2.5$  nm. Solid lines represent the measurements presented in Ref. 11 and the markers  $\circ$  display the results of the performed transport simulation.

metallic SWCNT's presented in Ref. 11. These measurements were carried out on individual nanotubes with Ohmic contacts that were grown on  $\text{SiO}_2/\text{Si}$  wafers.<sup>11</sup> The investigated SWCNT's have diameters  $d \sim 2-2.5$  nm and different lengths between  $L \sim 85$  nm and  $L \sim 700$  nm. We performed the transport calculations with the phonon energies  $\hbar\omega_1 = 160$  meV and  $\hbar\omega_2 = \hbar\omega_3 = 200$  meV, which are very close to the values reported in Ref. 15. The increment of the energy discretization was set to  $\Delta\varepsilon = 40$  meV. This guarantees that the phonon energies  $\hbar\omega_\eta$  are integer multiples of  $\Delta\varepsilon$  as supposed in Sec. III for an efficient treatment of the scattering operators. Following Ref. 15, we considered  $v_F = 8.4 \times 10^5$  m/s for the Fermi velocity. Regarding the group velocities of the optical phonon modes, we used  $v_1 = 5000$  m/s,  $v_2 = 2950$  m/s, and  $v_3 = 0$ . The velocity  $v_1$  of the zone-boundary phonons is slightly lower than the value of 7230 m/s obtained in Ref. 16 for  $\mathbf{q} = \mathbf{K}$ . At this symmetry point, however, the group velocity of K phonons takes on its maximum. The lower value of  $v_1 = 5000$  m/s used in the transport simulation is a good approximation of the  $q$ -averaged phonon velocity. For the relaxation times of the decay of optical phonons due to phonon-phonon interactions, we supposed  $\tau_\eta = 3.5$  ps for all optical phonon modes  $\eta = 1, 2, 3$ . This value is consistent with the anharmonic contribution to the linewidth of Raman  $G^\pm$  peaks ( $\gamma^{an} \sim 10$  cm<sup>-1</sup>) in metallic nanotubes.<sup>17</sup> The Ohmic contacts were treated as almost perfectly transmitting by assuming  $t_i^2 \sim 0.95$  for the transmission probabilities at the left ( $i=1$ ) and right ( $i=2$ ) contacts. The coefficients of the EPC were considered as the fitting parameters of the transport model. Concerning the elastic MFP of the electrons, we found  $l_e \sim 1000$  nm for the 700 nm long tube and  $l_e = 750$  nm for the shorter tubes. We mention that these results for the elastic MFP's are slightly higher than the 600 nm obtained in Ref. 11 and lower than the 1600 nm proposed in Refs. 12 and 13. The low-bias current, i.e.,  $U < 0.15$  V, is mainly controlled by the elastic MFP and the contact transmission. In the high-field region, the EPC parameters for the interaction of electrons with optical phonons play a dominant role. According to the DFT

calculations presented in Ref. 15, the coupling coefficients depend on the tube diameter via the scaling law

$$\gamma_\eta = \frac{v_F}{l_\eta} \frac{1}{d}, \quad (15)$$

with the constants  $l_1=92.0$  and  $l_2=l_3=225.6$ . Best agreement between the experimental and theoretical results was obtained by choosing  $d \sim 2.0\text{--}2.3$  nm in Eq. (15). Only in the case of  $L=700$  nm does the fitting of the results to the measured current-voltage curve reveal  $d \sim 3$  nm in Eq. (15). Since the diameters of the investigated SWCNT's are  $d \sim 2.0\text{--}2.5$  nm, the EPC coefficients determined by the transport calculations are consistent with the results of the DFT calculations<sup>15</sup> and the experimentally obtained values.<sup>16,17</sup> We note that the EPC constants  $\gamma_\eta$  are determined by the ground state of the electron-phonon system in the applied theory of lattice scattering<sup>22</sup> based on Eq. (4). These quantities can be calculated by applying DFT.<sup>15</sup> Far from equilibrium, the scattering rates and the MFP of electrons are modified due to the nonequilibrium behavior of the phonon distributions obtained from Eq. (8). In general, the coupling constants  $\gamma_\eta$  at high bias can differ from the equilibrium values as well. From the comparison of our fitting results for the EPC constants with the DFT results, we infer that the changes of  $\gamma_\eta$  play a minor role.

Figure 2 shows that the agreement between the measurements and theoretically obtained values is remarkably good in high- and low-field regions. We observe that the sudden drop of the conductance at  $U \sim 0.2$  V is accurately reproduced by the performed transport calculations. Furthermore, the theoretical results correctly reflect the increase of the high-field resistance for an increasing tube length  $L$ . In the case of  $L=700$  nm, the measured current is almost constant for  $U > 1.0$  V. This saturation effect is less pronounced in the theoretical results. However, we observe a significant population of electrons with energies  $\varepsilon > 0.5$  eV for very high applied voltages. Hence, scattering to higher semiconductor-like electron bands becomes important, which is neglected in the presented transport model. Since the velocity of the electrons in the higher bands is smaller than  $v_F$ , we expect that an increased population of these bands causes the observed saturation of the current.

### B. Nonequilibrium phonon effects

Our main aim is to investigate the influence of the nonequilibrium behavior of the optical phonons on the electron transport. These nonequilibrium phonon effects are quantified by comparing the results of the kinetic equations (2) and (8) with those of a transport model based on thermalized phonon distributions with adapted temperatures. The simulations relying on thermalized phonons are realized by replacing the actual phonon distribution functions  $g_\eta(q, x, t)$  by the corresponding equilibrium distributions

$$\langle g \rangle_\eta(x, t) = \frac{1}{N - \sigma_\eta} \sum_{m=1}^{N - \sigma_\eta} g_\eta(q_m^\eta, x, t) \quad (16)$$

for  $\eta=1, 2$  in each time step of our numerical scheme. We note that the integers  $\sigma_\eta$  introduced in Sec. III satisfy  $\hbar\omega_\eta$

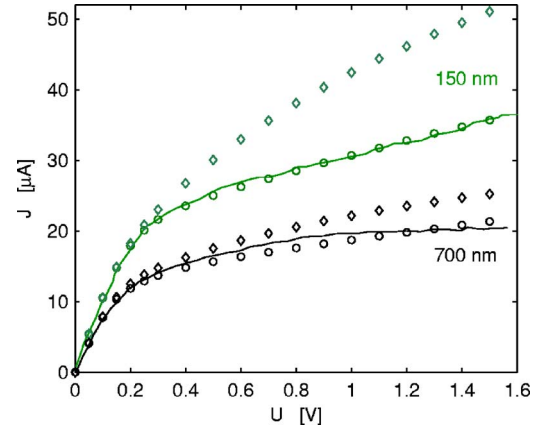


FIG. 3. (Color online) Influence of the nonequilibrium behavior of the optical phonons on the current-voltage characteristics (J-U) of metallic SWCNTs with  $L=700$  nm and  $L=150$  nm. The symbols  $\diamond$  display results obtained with equilibrium phonon distributions at adapted temperatures and the markers  $\circ$  represent results obtained with nonequilibrium phonons. Solid lines depict the experimental data presented in Ref. 11.

$= \sigma_\eta \Delta \varepsilon$ . The distribution functions defined by Eq. (16) provide the same number of phonons and therefore also the same phonon energy as the original distributions  $g_\eta(q, x, t)$  at all  $x$  and  $t$ . Moreover,  $\langle g \rangle_\eta(x, t)$  can be interpreted as the Bose-Einstein distribution with the effective temperature

$$T_\eta(x, t) = \frac{\hbar\omega_\eta}{k_B \log[1/\langle g \rangle_\eta(x, t) + 1]}. \quad (17)$$

The differences in the electron current obtained by considering either  $g_\eta(q, x, t)$  or  $\langle g \rangle_\eta(x, t)$  in the transport simulations are attributed to the impact of the nonequilibrium behavior of the optical phonon system. Such a comparison is presented in Fig. 3 for nanotubes with lengths  $L \sim 150$  nm and  $L \sim 700$  nm. We observe that the transport calculations based on thermalized phonon distributions overestimate the electron current significantly in the high-field regime. As expected the nonequilibrium phonon effects are more pronounced in short nanotubes in which higher electric fields arise. The deviations of the steady-state current reach up to 20% for  $L=700$  nm and more than 40% for  $L=150$  nm. It should be noted that the simulations relying on the equilibrium phonon distributions (16) already contain the heating effect of the phonon gas. In our algorithm, the Boltzmann equations (8) of the optical phonons are solved first and then the distribution functions  $g_\eta$  are replaced by  $\langle g \rangle_\eta$ . This replacement does not change the phonon energy, which guarantees a consistent description of the energy transfer from electrons to optical phonons and from optical phonons to the heat bath of acoustic phonons. Hence, the differences of the high-field current and conductance displayed in Fig. 3 are effects of the far-from-equilibrium dynamics of the optical phonons.

In order to study the nonequilibrium kinetics of the electron-phonon system in metallic SWCNT's at a microscopic level, we directly analyze the distribution functions. The deterministic numerical method presented in Sec. III al-

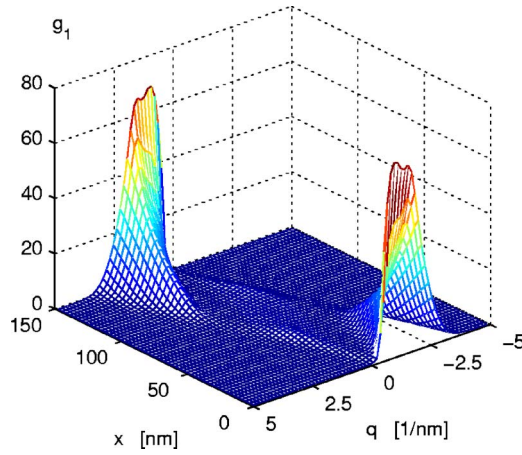


FIG. 4. (Color online) Steady-state results for a 150 nm long metallic SWCNT at 1 V bias: nonequilibrium distribution  $g_1$  of K phonons as function of  $x$  and  $q$ .

allows us to calculate the electron and phonon distributions in noise-free resolution. We consider a 150 nm long metallic SWCNT at a bias of  $U=1$  V. In Figs. 4 and 5, the steady-state distributions of K and  $\Gamma$  phonons are depicted as functions of the position variable  $x$  and the wave vector  $q$ . These results were obtained by taking into account the full dynamics of the optical phonons, i.e., by solving the systems (2) and (8). First, we notice the strong dependence of the phonon distribution functions on the phase-space variables which reflects the far-from-equilibrium situation. Two isolated peaks of the phonon occupations  $g_\eta$  occur at the boundaries of the tube. The maxima of the phonon distributions reach very large values of  $g_1 \sim 80$  and  $g_2 \sim 6$  compared to the equilibrium values  $g_1 \sim 2.1 \times 10^{-3}$  and  $g_2 \sim 4.4 \times 10^{-4}$  at  $T=300$  K. Furthermore, the phase-space distributions of the optical phonon modes are strongly anisotropic. At the left contact, e.g., the huge amount of K phonons with  $q < 0$  dominates the electron scattering while scattering processes with  $q > 0$  only play a minor role. This is an essential difference compared to thermalized phonon distributions, which are independent of the phonon wave vector, if constant phonon energies are as-

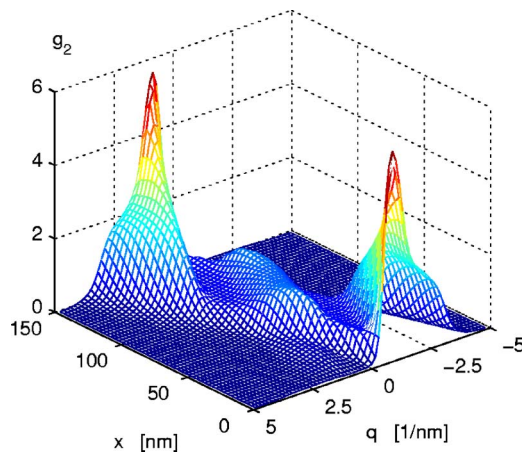


FIG. 5. (Color online) Steady-state results for a 150 nm long metallic SWCNT at 1 V bias: nonequilibrium distribution  $g_2$  of  $\Gamma$  phonons as function of  $x$  and  $q$ .

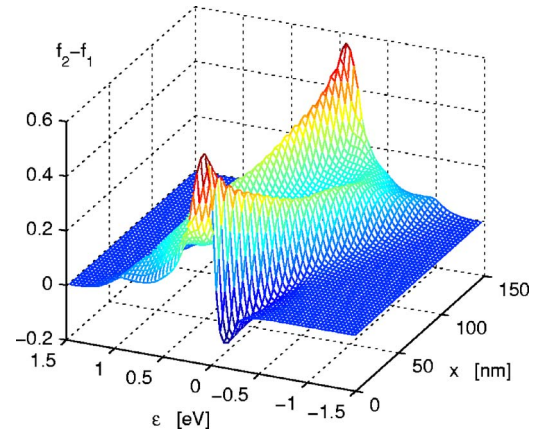


FIG. 6. (Color online) Steady-state results for a 150 nm long metallic SWCNT at 1 V bias: difference  $f_2 - f_1$  of the distribution functions of left and right propagating electrons interacting with nonequilibrium phonons as function of  $x$  and  $\epsilon$ .

sumed. The anisotropy of the phonon distribution results from an unbalanced number of left- and right-moving electrons with certain energies. According to the phonon scattering operators (9), phonons of mode  $\eta=1,2$  with wave vector  $q$  are emitted by electrons of type  $i=1,2$  with energy  $\epsilon_i^+ = \hbar(v_i q + \omega_\eta)/2$  and absorbed by those of type  $j \neq i$  with energy  $\epsilon_j^- = \hbar(v_j q - \omega_\eta)/2$ . Figure 6 shows the difference  $f_2 - f_1$  between the distribution functions of electrons with negative and positive velocity. The mesh plot exhibits a strong overshoot of left-propagating ( $i=2$ ) electrons with  $\epsilon > 0$  at the left and with  $\epsilon < 0$  at the right contact. Since  $\epsilon_2^+ = \hbar(v_2 q + \omega_\eta)/2$  and  $v_2 = -v_F$ , these electrons mainly emit optical phonons with  $q < 0$  ( $q > 0$ ) at  $x \sim 0$  ( $x \sim L$ ). Therefore, an accumulation of optical phonons arises at the boundaries of the nanotube.

The special structure of the phonon distributions displayed in Fig. 4 and 5 also explains the observed sensitivity of the electron current on the phonon velocities  $v_\eta$ . At first glance, this effect seems to be surprising, since the velocities  $v_1 \sim 5$  km/s and  $v_2 \sim 3$  km/s are two orders of magnitude smaller than the electron velocity  $v_F = 8.4 \times 10^5$  m/s. However, the performed calculations show that most of the optical phonons are emitted close to the boundaries (see Figs. 4 and 5). Due to the positive dispersions,<sup>16</sup> i.e.,  $\pm v_\eta > 0$  for  $\pm q > 0$ , the phonons only need a short time to reach the contacts which are treated as perfectly absorbing. As a consequence, larger phonon velocities lead to decreased rates of back scattering and increased electron currents in the high-field regime.

Regarding the electron distribution functions, it should be pointed out that the difference  $f_2 - f_1$  plotted in Fig. 6 is larger than zero even for energies  $|\epsilon| > 0.5$  eV. This indicates that a significant amount of electrons with energies  $|\epsilon| > 0.5$  eV exist that contribute to the total current. For the considered nanotube with  $L=150$  nm and an applied bias of  $U=1.0$  V, this contribution is  $\sim 20\%$ . Hence, we suggest that the scattering of electrons to the nonlinear semiconductorlike subbands becomes important for applied voltages  $U \geq 1.0$  V.

In Fig. 7 we plot the steady-state distributions  $\langle g \rangle_\eta(x)$  obtained from a transport simulation based on the equilib-

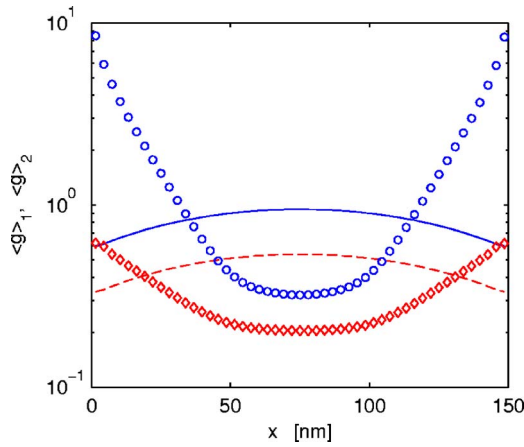


FIG. 7. (Color online) Steady-state results for a 150 nm long metallic SWCNT at 1 V bias: distributions  $\langle g \rangle_1$  and  $\langle g \rangle_2$  of thermalized K phonons (solid line) and  $\Gamma$  phonons (dashed line) as functions of  $x$ ;  $q$ -averaged nonequilibrium distributions of K phonons (symbols  $\circ$ ) and  $\Gamma$  phonons (symbols  $\diamond$ ) as functions of  $x$ .

rium phonon distributions defined in Eq. (16). Again, the values of  $\langle g \rangle_\eta(x)$  were adapted according to Eq. (16) in each time step of the numerical scheme. To compare the results with those of the simulation including nonequilibrium phonon effects, we display the  $q$ -averages (16) of the steady-state nonequilibrium phonon distributions  $g_1(q, x)$  and  $g_2(q, x)$  with the symbols  $\circ$  and  $\diamond$  in Fig. 7. We obtain a completely different behavior of the optical phonon systems in the two situations. The thermalized phonon occupations exhibit maxima at the midpoint of the nanotube in contrast to the high peaks of the nonequilibrium phonon distributions arising at the boundaries. Also, the dependence of the effective equilibrium distributions on the spatial variable  $x$  is much weaker than in the case of nonequilibrium phonons. It should be noted that the scattering operators (5), (9), and (10) couple the Boltzmann equations of electrons (2) and optical phonons (8) with each other in a nonlinear way. To realize the assumption of thermalized phonon distribution, we replace  $g_1$  and  $g_2$  by their corresponding averages  $\langle g \rangle_1$  and  $\langle g \rangle_2$ . This procedure modifies the rates of electron back-scattering processes and changes the electron distribution functions  $f_i$ . The modified electron distributions re-affect the temporal evolution of the optical phonon distributions. Finally, the coupled system of electrons and thermalized phonons approaches a stationary state very different from that of electrons and nonequilibrium phonons.

The difference  $f_2 - f_1$  of the phase-space distributions of left- and right-moving electrons obtained by assuming thermalized phonon distributions is depicted in Fig. 8. Compared to the result of the calculation including nonequilibrium phonons presented in Fig. 6, the difference  $f_2 - f_1$  takes on larger values, especially for  $\varepsilon \in [0.2, 0.8]$  eV at  $x \sim 0$  and for  $\varepsilon \in [-0.8, -0.2]$  eV at  $x \sim L$ . These electrons are very efficiently scattered back by the large amount of nonequilibrium phonons created at the boundaries (see Figs. 4, 5, and 7). As a consequence,  $f_2 - f_1$  is reduced, if far-from-equilibrium phonon effects are taken into account. The electron current  $J(x, t)$  is obtained from the difference  $f_2 - f_1$  by performing the integral

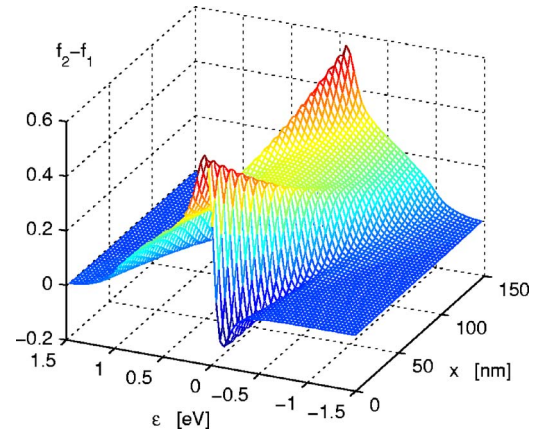


FIG. 8. (Color online) Steady-state results for a 150 nm long metallic SWCNT at 1 V bias: difference  $f_2 - f_1$  of the distribution functions of left- and right-propagating electrons interacting with thermalized phonons as function of  $x$  and  $\varepsilon$ .

$$J(x, t) = \frac{4e_0}{h} \int_{\mathbb{R}} d\varepsilon [f_2(\varepsilon, x, t) - f_1(\varepsilon, x, t)]. \quad (18)$$

The larger values of  $f_2 - f_1$  obtained in the case of thermalized phonon distributions imply a larger electron current as shown in Fig. 3.

The results presented so far clearly show that nonequilibrium phonons strongly influence the electron current in sub-micron SWCNT's at high applied bias. Descriptions of the optical phonon system based on thermalized distributions with adapted temperatures fail in such situations. Due to the significant impact of nonequilibrium phonons, the high-field transport properties of metallic SWCNT's depend on the anharmonic lifetimes  $\tau_\eta$  of the optical phonons. Figure 9 displays the current-voltage characteristics of a 300 nm long nanotube obtained for different values of the phonon relaxation times  $\tau_\eta$ . We observe a very strong dependence of the current on  $\tau_\eta$  in the high-field region, whereas  $\tau$  has no influence on the current for  $U < 0.15$  V. In the case of  $\tau = 0$ ,

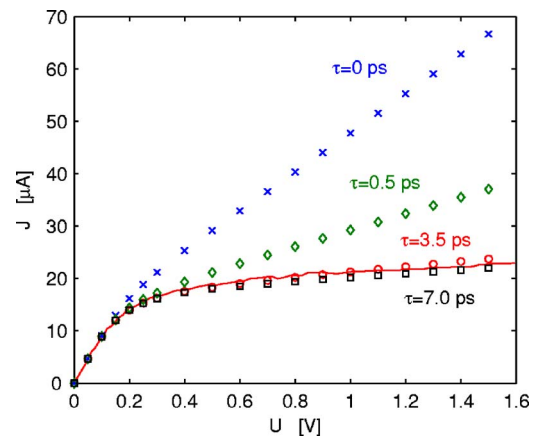


FIG. 9. (Color online) Current-voltage ( $J$ - $U$ ) characteristics of a 300 nm long ohmically contacted SWCNTs with diameter  $d = 2$  nm calculated for different phonon relaxation times  $\tau$ . The solid line represents the experimental data presented in Ref. 11.

any deviations of the phonon distributions  $g_\eta$  from the Bose-Einstein distributions  $g_\eta^0$  are removed instantaneously by phonon-phonon interaction processes. This means that the optical phonon system is kept in equilibrium at the ambient temperature  $T$  for all times. The high-field current obtained under this assumption is  $\sim 2-3$  times larger than the measured results. The high-field conductance  $G=dJ/dV$  for  $\tau_\eta=0$  is  $\sim 7-8$  times larger than that obtained with  $\tau_\eta=3.5$  ps. By increasing the phonon lifetime, the nonequilibrium phonon distributions are built up and the optical MFP of the electrons is reduced. Hence, we obtain lower electron currents for larger  $\tau_\eta$ . At  $\tau=3.5$  ps the calculated current agrees well with the measurements. A further increase of the relaxation time due to phonon-phonon interactions hardly changes the electron current (see the results obtained for  $\tau_\eta=7.0$  ps). Our calculations show that the temporal evolution of the electron-phonon system approaches a stationary state within  $\sim 10-20$  ps in the high-field regime. After a time span of  $\sim 7$  ps, the temporal changes of the current are smaller than 0.2% for an applied bias of  $U=1.0$  V. Therefore, we observe no further reduction of the steady-state results for increased relaxation times  $\tau_\eta$ . It should be mentioned that the time interval to reach the stationary state is larger for longer tubes. Hence, also the impact of the relaxation time on the current depends on the tube length  $L$ . We point out that using the relaxation time  $\tau_\eta=3.5$  ps estimated from the Raman  $G^\pm$ -peak measurements<sup>17</sup> leads to a very good agreement of the results with the experimental data for all investigated tubes with lengths between 85 nm and 700 nm (see Fig. 2).

## V. CONCLUSIONS

We have studied theoretically the influence of hot phonons on the high-field transport properties of metallic SWCNT's. The performed investigations rely on deterministic numerical solutions of a coupled system of Boltzmann equations of electrons and optical phonons. In this way the nonequilibrium dynamics of the optical phonons is taken into account. Fitting the results of the transport simulations to measured current-voltage characteristics reveals EPC coefficients that are consistent with those determined experimen-

tally and obtained from DFT calculations. We demonstrate that the distributions of  $\Gamma$  and K phonons in carbon nanotubes are driven far from equilibrium at high bias. The steady-state phonon occupations are strongly anisotropic and especially high at the boundaries of the tubes. This large number of optical phonons significantly reduces the optical MFP's compared to the situation of thermal equilibrium. Moreover, the actual shape of the phonon distributions strongly influences the steady-state current. It is shown that transport models based on thermalized phonon systems with adapted temperatures are not adequate for describing the nonequilibrium kinetics of the coupled electron-phonon system in SWCNT's at high bias. Furthermore, we demonstrate that the high-field current is sensitive to the temporal relaxation of the optical phonons caused by phonon-phonon interactions.

Such interaction processes are of special interest for studying the self-heating in suspended nanotubes and the related negative conductance phenomena. The presented kinetic equations can be considered as a starting point to derive a suitable transport model for suspended SWCNT's. Due to the dynamical treatment of the optical phonons in our model, we directly obtain their nonequilibrium distributions. This information can be used to determine the self-heating of the nanotube, i.e., to calculate the time- and space-dependent temperature of the acoustic phonons. A kinetic approach to this problem requires an additional Boltzmann equation for acoustic phonons, which is coupled with those for electrons and optical phonons. The corresponding coupling terms must take into account electron-phonon interactions as well as interactions between optical and acoustic phonons. These interaction mechanisms between optical and acoustic phonons especially deserve further investigation.

## ACKNOWLEDGMENTS

The authors are indebted to A. M. Anile of the Dipartimento di Matematica e Informatica, Università di Catania, Italy, for drawing their attention to the investigated problem. This work has been supported by the Fond zur Förderung der wissenschaftlichen Forschung, Vienna, under Contract No. P17438-N08.

\*Electronic address: auer@itp.tu-graz.ac.at

†Electronic address: schuerr@itp.tu-graz.ac.at

‡Electronic address: Christian.Ertler@physik.uni-regensburg.de

<sup>1</sup>M. S. Dresselhaus, G. Dresselhaus, and A. Jorio, *Annu. Rev. Mater. Res.* **34**, 247 (2004).

<sup>2</sup>M. Fuhrer, H. Park, and P. L. McEuen, *IEEE Trans. Nanotechnol.* **1**, 78 (2002).

<sup>3</sup>P. Avouris, J. Appenzeller, R. Martel, and S. Wind, *Proc. IEEE* **91**, 1772 (2002).

<sup>4</sup>A. Javey, J. Guo, D. B. Farmer, Q. Wang, D. Wang, R. G. Gordon, M. Lundstrom, and H. Dai, *Nano Lett.* **4**, 447 (2004).

<sup>5</sup>C. T. White and T. N. Todorov, *Nature (London)* **393**, 240 (1998).

<sup>6</sup>A. Javey, J. Guo, Q. Wang, M. Lundstrom, and H. Dai, *Nature (London)* **424**, 654 (2003).

<sup>7</sup>S. J. Tans, A. R. M. Verschueren, and C. Dekker, *Nature (London)* **386**, 474 (1997).

<sup>8</sup>W. Liang, M. Bockrath, D. Bozovic, J. H. Hafner, M. Tinkham, and H. Park, *Nature (London)* **411**, 665 (2001).

<sup>9</sup>J. Kong, E. Yenilmez, T. W. Tomblor, W. Kim, H. Dai, R. B. Laughlin, L. Liu, C. S. Jayanthi, and S. Y. Wu, *Phys. Rev. Lett.* **87**, 106801 (2001).

<sup>10</sup>Z. Yao, C. Kane, and C. Dekker, *Phys. Rev. Lett.* **84**, 2941 (2000).

<sup>11</sup>A. Javey, J. Guo, M. Paulsson, Q. Wang, D. Mann, M. Lundstrom, and H. Dai, *Phys. Rev. Lett.* **92**, 106804 (2004).

- <sup>12</sup>J.-Y. Park, S. Rosenblatt, Y. Yaish, V. Sazonova, H. Üstünel, S. Braig, T. A. Arias, P. Brouwer, and P. L. McEuen, *Nano Lett.* **4**, 517 (2004).
- <sup>13</sup>E. Pop, D. Mann, J. Cao, Q. Wang, K. Goodson, and H. Dai, *Phys. Rev. Lett.* **95**, 155505 (2005).
- <sup>14</sup>D. Mann, E. Pop, J. Cao, Q. Wang, K. Goodson, and H. Dai, *J. Phys. Chem. B* **110**, 1502 (2006).
- <sup>15</sup>M. Lazzeri, S. Piscanec, F. Mauri, A. C. Ferrari, and J. Robertson, *Phys. Rev. Lett.* **95**, 236802 (2005).
- <sup>16</sup>S. Piscanec, M. Lazzeri, F. Mauri, A. C. Ferrari, and J. Robertson, *Phys. Rev. Lett.* **93**, 185503 (2004).
- <sup>17</sup>M. Lazzeri, S. Piscanec, F. Mauri, A. C. Ferrari, and J. Robertson, cond-mat/0508700 (unpublished).
- <sup>18</sup>J. C. Vaissiere, J. P. Nougier, M. Fadel, L. Hlou, and P. Kocevar, *Phys. Rev. B* **46**, 13082 (1992).
- <sup>19</sup>J. C. Vaissiere, J. P. Nougier, L. Varani, P. Houlet, L. Hlou, L. Reggiani, and P. Kocevar, *Phys. Rev. B* **53**, 9886 (1996).
- <sup>20</sup>C. Auer, W. Koller, and F. Schürer, *SIAM J. Appl. Math.* **64**, 1457 (2004).
- <sup>21</sup>M. Galler and F. Schürer, *J. Phys. A* **37**, 1479 (2004).
- <sup>22</sup>B. K. Ridley, *Quantum Processes in Semiconductors* (Oxford University Press, Oxford, 1999).
- <sup>23</sup>M. Lundstrom, *Fundamentals of Carrier Transport* (Cambridge University Press, Cambridge, 2000).
- <sup>24</sup>C. Jacoboni and P. Lugli, *The Monte Carlo Method for Semiconductor Device Simulation* (Springer, Wien, 1989).
- <sup>25</sup>M. V. Fischetti, *IEEE Trans. Electron Devices* **38**, 634 (1991).
- <sup>26</sup>J. A. Carrillo, I. M. Gamba, A. Majorana, and C.-W. Shu, *J. Comput. Phys.* **184**, 498 (2003).
- <sup>27</sup>C. Ertler and F. Schürer, *J. Phys. A* **36**, 8759 (2003).
- <sup>28</sup>G. Jiang and C.-W. Shu, *J. Comput. Phys.* **126**, 202 (1996).
- <sup>29</sup>C.-W. Shu and S. Osher, *J. Comput. Phys.* **77**, 439 (1988).